Modulation Scheme Analysis for Low-Power Leadless Pacemaker Synchronization Based on Conductive Intracardiac Communication

Adrian Ryser, Tobias Schmid, Lukas Bereuter, Jürgen Burger, Tobias Reichlin, Thomas Niederhauser, *Member, IEEE*, and Andreas Haeberlin

***Abstract*—Conductive intracardiac communication (CIC) has been demonstrated as a promising concept for the synchronization of multi-chamber leadless cardiac pacemakers (LLPMs). To meet the 2–5 μW power budget of a LLPM, highly specialized CIC-transceivers, which make optimal use of the cardiac communication channel, need to be developed. However, a detailed investigation of the optimal communication parameters for CIC-based LLPM synchronization is missing so far. This work analyzes the intracardiac communication performance of two low-power modulation techniques, namely On-Off-Keying (OOK) and Manchester-encoded baseband transmission (BB-MAN), as a function of the transmitted bit-energy. The bit error rate (BER) of a prototype dual-chamber LLPM was determined both in simulation and in-vitro experiments on porcine hearts. A BER of 1e−4 was achieved with a median bit-energy in the range of 3-16 pJ (interquartile range: 4-15 pJ) for data rates from 75-500 kbps and a receiver input noise density of 7 nV/$\sqrt{\text{Hz}}$. Both modulation schemes showed comparable performance, with BB-MAN having a slight bit-energy advantage (1-2 dB at 150-500 kbps) under equalized transceiver characteristics. This study demonstrates that reliable CIC-based LLPM synchronization is feasible at transmitted power levels <10 nW under realistic channel conditions and receiver noise performance. Therefore, modulation techniques such, as BB-MAN or OOK, are preferable over recently proposed alternatives, such as pulse position modulation or conductive impulse signaling, since they can be realized with fewer hardware resources and smaller bandwidth requirements. Ultimately, a baseband communication approach might be favored over OOK, due to the more efficient cardiac signal transmission and reduced transceiver complexity.**

***Index Terms*—Baseband transmission, conductive intracardiac communication, galvanic-coupled conductive communication, intra-body communication, leadless CRT, leadless dual-chamber pacing, leadless pacemaker, Manchester code, modulation scheme, multisite pacing, On-Off-Keying, OOK.**

I. Introduction

WITH over 1 million implantations per year, conventional cardiac pacemakers (PMs) are well established medical devices for the treatment of bradyarrhythmias [1]. Recently, leadless pacemakers (LLPMs) have been introduced to overcome the major sources of complications in conventional PMs, which are related to the pacing leads [2], [3]. LLPM implantation is safe and effective if proper implantation techniques are used [4]. However, currently available LLPMs, which are single-chamber systems implanted in the right ventricle, suffer from two main limitations. The majority of PM patients requires atrio-ventricular (AV) synchronous ventricular stimulation (i.e. that the ventricular pacing is synchronized to the intrinsic atrial rhythm) and/or additional atrial pacing. Although the recently introduced Micra AV TPS (Medtronic, USA) LLPM, which provides contactless atrial sensing and tracking, successfully achieves AV synchronous pacing with a single device, its performance is still considerably worse than that of conventional dual-chamber PMs [5].

As an alternative, multiple LLPMs, that wirelessly synchronize their activity, could be implanted in different chambers to overcome the above mentioned limitations [6], [7]. However, device synchronization remains a challenge, due to the significant constraints on the corresponding hardware in terms of power consumption and size. Radio frequency (RF) communication

Manuscript received February 14, 2022; revised April 4, 2022; accepted May 6, 2022. Date of publication May 27, 2022; date of current version July 14, 2022. This work was supported by the Swiss Heart Foundation, the Hasler Foundation, the Novartis Foundation (grants to A. Haeberlin) and the sitem-insel support funds (Grant to T. Reichlin). This paper was recommended by Associate Editor H. Jiang. *(Corresponding author: Adrian Ryser.)*

Adrian Ryser is with the Sitem Center for Translational Medicine and Biomedical Entrepreneurship, University of Bern, 3010 Bern, Switzerland, with the Institute for Human Centered Engineering HuCE, Bern University of Applied Sciences, 2501 Biel, Switzerland, with the Department of Cardiology, Inselspital, Bern University Hospital, University of Bern, 3010 Bern, Switzerland, and also with the ARTORG Center for Biomedical Engineering Research, University of Bern, 3008 Bern, Switzerland (e-mail: adrian.ryser@sitem.unibe.ch).

Tobias Schmid and Tobias Reichlin are with the Department of Cardiology, Inselspital, Bern University Hospital, University of Bern, 3010 Bern, Switzerland (e-mail: tobias.schmid@gmx.ch; tobias.reichlin@insel.ch).

Lukas Bereuter is with the ARTORG Center for Biomedical Engineering Research, University of Bern, 3008 Bern, Switzerland (e-mail: lukas.bereuter@artorg.unibe.ch).

Jürgen Burger is with the Sitem Center for Translational Medicine and Biomedical Entrepreneurship, University of Bern, 3010 Bern, Switzerland (e-mail: juergen.burger@med.unibe.ch).

Thomas Niederhauser is with the Sitem Center for Translational Medicine and Biomedical Entrepreneurship, University of Bern, 3010 Bern, Switzerland, and also with the Institute for Human Centered Engineering HuCE, Bern University of Applied Sciences, 2501 Biel, Switzerland (e-mail: thomas.niederhauser@bfh.ch).

Andreas Haeberlin is with the Sitem Center for Translational Medicine and Biomedical Entrepreneurship, University of Bern, 3010 Bern, Switzerland, with the Department of Cardiology, Inselspital, Bern University Hospital, University of Bern, 3010 Bern, Switzerland, and also with the ARTORG Center for Biomedical Engineering Research, University of Bern, 3008 Bern, Switzerland (e-mail: andreas.haeberlin@insel.ch).

This article has supplementary material provided by the authors and color versions of one or more figures available at https://doi.org/10.1109/TBCAS.2022.3178444.

Digital Object Identifier 10.1109/TBCAS.2022.3178444

seems not suitable for this task, due to the high signal absorption in the human body and the low antenna impedance requiring large transmitted power levels [7], [8]. Galvanic-coupled conductive intracardiac communication (CIC) has been proposed as a low-power alternative, due to the relatively low channel attenuation and the utilization of low-frequency signals in the 1 kHz to 20 MHz range [6], [9]–[12]. While feasibility of CIC-based synchronization has recently been demonstrated, the presented systems required extensive hardware and power consumption resources [6], [9], [12].

In a typical dual-chamber LLPM system, one device would be located in the right atrium and one in the right ventricle of the heart, respectively. Both devices would need to synchronize their activity periodically by communicating over the intracardiac channel. The total power consumption P_{tot} of such transceivers can be described by

$$P_{tot} = P_{TX} + P_{cir} = N_{bps} \cdot E_{bit} + P_{cir}, \tag{1}$$

where P_{TX} is the transmitted power applied to the cardiac channel and P_{cir} summarizes the power consumption of the electronic circuits. P_{TX} can be re-written as the energy per bit E_{bit} times the mean number of bits N_{bps}, transmitted every second. A key challenge of LLPM synchronization is to achieve a sufficiently low bit error rate (BER) during transmission, to guarantee synchronous pacing, while operating on power levels substantially lower compared to the overall 2-5 μW budget of a LLPM.

Previous studies on LLPM synchronization reported the achieved communication performance in terms of BER and P_{TX}, however, an analysis of influencing factors such as channel attenuation, channel impedance and transceiver performance was lacking [6], [9], [12]. To design a power-optimized transceiver, a detailed understanding of the major influencing factors on communication reliability and transmitted power consumption is crucial, as minimizing P_{tot} will require an optimal trade-off between BER, P_{cir} and P_{TX}.

An important aspect of any communication system is the employed modulation technique used to encode the transmitted data. In previous studies, modulation schemes which try to minimize P_{TX}, such as pulse position modulation (PPM) and conductive impulse signaling (CIS), have been proposed [6], [9], [12]. The authors demonstrated that reliable communication is feasible at $P_{TX} < 1$ μW, transmitting a reasonable amount of bits for the given application. However, for a power-optimized synchronization, the impact of the modulation scheme on the transceiver circuits should be considered as well. While PPM and CIS could represent a beneficial choice in case P_{tot} is dominated by P_{TX}, they suffer from relevant drawbacks. Considering PPM, the required receiver bandwidth, for a given data rate and a fixed number of carrier cycles per slot, is increased compared to other modulation schemes [13]. In addition, symbol and frame synchronization are more complex, since only a few signal pulses per message are sent at irregular intervals [14]. Similarly, receiving wideband pulses in CIS, requires a large input bandwidth and high sampling frequencies, which are orders of magnitude above the data rate used [12]. These factors may considerably increase circuit complexity and bandwidth, and, consequently, rise P_{cir}.

Although the miniaturization of the electronics in a future application-specific-integrated-circuit (ASIC) will allow to reduce P_{cir}, compared to the presented systems, it may still remain the dominating factor. In this case, modulation schemes with the potential to reduce P_{cir}, might represent a crucial design factor [15]. Therefore, two low-complexity modulation schemes, namely On-Off-Keying (OOK) and baseband transmission with Manchester encoding (BB-MAN), have been considered in this work (more details on the selection of these modulation techniques are given in the methods section).

In this work we aim to analyze the required bit-energy E_{bit} to achieve reliable communication, by considering key factors, such as the electrical properties of the CIC channel, the choice of the modulation scheme, the communication frequency, and the electronic performance of the transceiver. An optimized receiver, suitable for miniaturization in a low-power integrated circuit, was developed. The BER performance of a LLPM prototype was assessed during in-vitro experiments on porcine hearts and blood. In addition, a simulation model of the intracardiac communication was developed and used to predict the BER performance as function of the most important system parameters.

II. Methods

For each investigated in-vitro configuration, three separate measurements were performed to obtain the BER performance, the transfer function and the inter-electrode impedance, respectively. The BER was measured separately for each modulation scheme and data rate combination. In addition, one simulation was performed for each BER measurement, based on the corresponding transfer function and impedance measurements.

In the subsections below the selection of the modulation schemes and communication parameters, as well as the electronic prototypes, the measurement setup, the in-vitro experiments and the simulation model are discussed in detail.

A. Modulation Scheme & Communication Parameters

Two requirements were considered when selecting the modulation scheme and communication frequency. Firstly, the communication signal should be direct current (DC) free. The resulting net charge at the electrode-tissue interface is almost zero, which prevents tissue damage and increasing the polarization impedance and, thus, the pacing threshold. Secondly, the communication signal should not lead to myocardial capture to prevent accidental pacing during synchronization.

For passband modulation with a sinusoidal carrier the first requirement is not a concern. On-Off-Keying modulation with non-return-to-zero (NRZ) encoding was selected from this category, since it can be implemented with ultra-low-power circuit designs, as recently demonstrated [16]–[19].

For baseband communication with rectangular pulses, the DC component can be eliminated by using either a constant-weight code, a paired disparity code or a scrambler. The latter two approaches achieve zero DC offset, by balancing the pulse polarities over multiple bits. In contrast, Manchester encoding

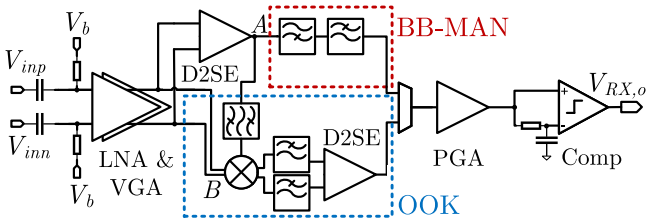

Fig. 1. Principal schematic of the receiver prototype.

(BB-MAN), representing a constant-weight code, eliminates the DC component at the bit level. Since for LLPM synchronization the total amount of bits per message is low, BB-MAN was used during this study. Manchester code uses twice the bandwidth, for a given data rate, compared to the NRZ encoding adopted for OOK.

Previous work has found good cardiac signal transmission in the frequency range from 10 kHz to 20 MHz [10], [11]. Considering patient safety, signal transmission and transceiver power consumption, the four data rates of 75 kbps, 150 kbps, 300 kbps, and 500 kbps were investigated in this work. The OOK carrier frequency f_{car} was set one decade higher relative to the data rate, i.e. in the range between 750 kHz and 5 MHz.

B. Electronic Prototypes

The analog parts of a CIC-based receiver (RX) and transmitter (TX) prototype were developed in the form of two separate evaluation boards, based on discrete electronic components.

1) Receiver: A circuit schematic of the receiver can be found in Fig. 1. The capacitor and DC-bias resistor at both differential inputs form a first-order high-pass filter (HPF). The cut-off frequency of the HPF is set to 3 kHz to suppress low-frequency physiological signals without significant impact on the high-frequency communication signal. While the two signal paths for processing the OOK and BB-MAN signals share the same input and output stages, separate circuits for demodulation and filtering have been implemented. The input stage is split up into a low-noise amplifier (LNA), achieving a moderate gain of 5, and a voltage-controlled variable gain amplifier (VGA), providing up to 80 dB of gain at a fixed 3-dB bandwidth of 18 MHz (AD8338, Analog Devices, USA). The offset-nulling feature of the VGA is activated and its inputs are AC-coupled to suppress the propagation of the LNA offset. At a maximum gain of 80 dB the LNA and the VGA achieve a DC-offset of 2 mV and 45 mV, respectively. The LNA and VGA together realize a flat frequency characteristic from 10 kHz to 10 MHz, in order to identically amplify the BB-MAN and the OOK signals. The LNA was designed to have a relatively high input impedance $Z_{in} = (23\,\mathrm{k\Omega} \parallel 1\,\mathrm{pF})$, to have a negligible impact on the channel attenuation over the entire frequency range used in this study [11]. Following amplification the differential BB-MAN signal is converted to single-ended and filtered by a second-order composite band-pass filter. Both the LPF and the HPF of this stage, are realized in a Sallen-Key topology and the cut-off frequencies can be selected based on the data rate.

The OOK signal is demodulated with a synchronous detector based on a balanced modulator circuit. The sinusoidal input signal is mixed with an amplified and band-pass filtered version of itself, leading to a rectified waveform. The output signal is passed through a programmable RC LPF to retrieve the baseband waveform and to remove high frequency mixing products. The gain of the preceding stages is chosen such that amplitudes of at least 50 mV and 500 mV are present at the signal and carrier inputs of the mixer, respectively. A high carrier amplitude ensures complete and fast switching of the mixer. The mixer noise can consequently be minimized and, thus, has a negligible effect on the signal-to-noise-ratio (SNR) of the communication signal.

The BPF filter in the mixer path is designed with a second-order Sallen-Key topology and variable central frequency. The Q-factor is fixed to a value of 3, providing sufficient out-of-band filtering such that the switching of the mixer is not compromised by noise and disturbances. At the same time the BPF has a fast response time with respect to the data rate. Therefore, significant phase shifts between the two mixer inputs are avoided, even in case of a slight misalignment of the central frequency and f_{car}.

The output circuits, consisting of a programmable gain amplifier (PGA) and a comparator, are shared by both signal paths, as well. The PGA allows setting the input voltage of the comparator to a sufficient level, guaranteeing a negligible propagation delay compared to the data rate. The slicing comparator operates as a 1-bit analog-to-digital converter and realizes the baseband bit stream output. The reference voltage input of the comparator is set to half of the two analog voltage levels representing bit 1 and bit 0.

2) Transmitter: The transmitter is realized with the arbitrary waveform generator (AWG) of a Handyscope HS5 (TiePie engineering, Netherlands) combined with a custom-made differential output driver (based on the LT1994 fully-differential amplifier), providing a balanced signal to the TX electrodes. For each modulation technique an individual AWG waveform based on the same random bit sequence $b_{n,TX}$ and with a resolution of 400 points per bit, was generated in MATLAB R2020a (MathWorks, USA).

C. In-Vitro Setup

1) Electrodes: The receiver and transmitter electronics were connected to porcine hearts using pairs of epicardial needle electrodes. The stainless steel needles were soldered to a printed-circuit-board (PCB). The inter-electrode distance was 15 mm. The electrode length was 10 mm, to ensure that the needles can penetrate the myocardium and are in contact with the blood inside the heart chambers.

To represent a typical dual-chamber configuration, one electrode PCB was sutured epicardially on the right atrium (RA) and the right ventricle (RV), respectively (cf. Fig. 2). The electrode distance was set between 60 mm to 70 mm, representing a reasonable separation of two endocardial LLPMs. For each sample, three RV electrode orientations with respect to the fixed RA electrode were analyzed. In the 0° configuration the two electrode PCBs were placed in parallel. For the other two configurations the RV electrode was rotated by 30° and 60°, respectively, while keeping the midpoint distance to the RA electrode constant.

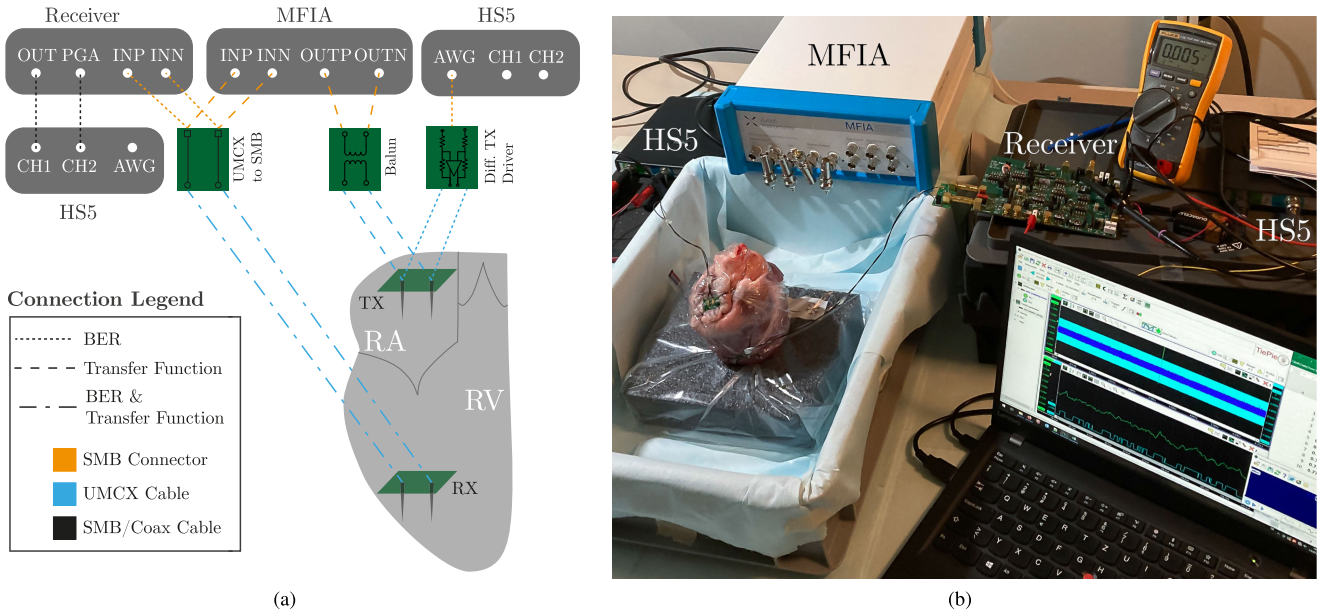

Fig. 2. Schematic (a) and photograph (b) of the setup used to measure the BER performance and the channel transfer function (see connection legend). The RX electrodes, sutured to the right ventricle of the porcine heart located in the middle of (b), were connected to the receiver prototype PCB. The two Handyscope HS5 devices were used to generate and record the bit streams. The MFIA was used to measure the inter-electrode impedance and the transfer function.

2) Samples: The porcine heart and blood samples were obtained from adult domestic pigs (weight 90-120 kg) collected freshly at the slaughterhouse. To prevent clotting, the blood was heparanized (5000 U/l) directly after being extracted from the animal within 1-2 minutes after death. The experiments were subsequently performed within the next 5-60 hours. A total of five in-vitro samples, three without blood and two with blood filled into the RA and RV, were measured.

D. Measurements

1) Bit Error Rate Measurement: A schematic and a photograph of the BER measurement setup are shown in Fig. 2. At both, the transmitter and the receiver, a Handyscope HS5 device was used to generate and record the communication signal, respectively. The laptops connected to the Handyscopes, were battery-powered to avoid parasitic coupling through the measurement equipment or the powerline [20], [21]. To further minimize the parasitic coupling of the TX and RX signals through the environment, a fully differential signal path was used and the electrodes were connected to the transmitter and the receiver, respectively, with coaxial cables. In addition, sensitive signal lines on the PCBs were kept as short as possible and shielded by ground planes/lines. The generation and propagation of spurious common-mode (CM) signals and their conversion into differential signals was minimized by the subsequent measures. Firstly, a balanced driver, with a minimum differential output matching of 56 dB over the frequency range from 1 kHz to 5 MHz, was used at the transmitter. Secondly, the parasitic coupling capacitance between the TX and RX ground potentials was minimized by separating the receiver and transmitter electronics as far as possible from each other. Lastly, to suppress any remaining CM signal at the receiver, a differential input stage with a minimum common-mode-rejection-ratio (CMRR) of 50 dB was employed (cf. Section II-B for more details on the prototypes). The transmitter amplitude V_{TX} was varied to cover a target BER range from 1e−6 to 1e−1. A sequence of one million bits $b_{n,RX}(V_{TX})$ was recorded at the receiver for each V_{TX} step. The filters and the gain of the receiver were adjusted according to the data rate f_{data} and the signal amplitude. For OOK, the LPF cut-off frequency and the BPF central frequency were adjusted to f_{data} and f_{car}, respectively. For BB-MAN, occupying twice the bandwidth, the LPF cut-off frequency was set to $2 \cdot f_{data}$.

As depicted in Fig. 3(a), BER(V_{TX}) was determined by comparing the received bit-stream $b_{n,RX}(V_{TX})$ to the transmitted bit sequence $b_{n,TX}(V_{TX})$ in post-processing. Lastly, the BER was expressed as a function of bit-energy (i.e. BER(E_{bit})), by calculating E_{bit} from V_{TX} and the transmitter inter-electrode impedance Z_{RA} (cf. Fig. 3(a) and Section II-E3).

2) Impedance and Transfer Function Measurement: The inter-electrode impedance and the transfer function were measured with the MFIA impedance analyzer (Zurich Instruments, Switzerland) in the frequency range from 1 kHz to 5 MHz.

For the transfer function measurements the MFIA was operated with differential inputs and outputs. A custom-made balun board (PWB2010 L, Coilcraft, USA) was inserted in series with the output to galvanically isolate the signal generator and the spectrum analyzer of the MFIA (cf. Fig. 2(a)). Additionally, this helped a) to minimize parasitic coupling inside and outside the MFIA, arising due to the inevitable proximity of the TX and RX signals and b) to suppress the propagation of unwanted CM signals. The number of baluns and their location in the setup has to be carefully considered, to realize an undistorted measurement of the intracardiac attenuation. A single balun at the TX site was used, since it has been demonstrated that such a configuration closely matches a battery-powered measurement system with separate transmitter and receiver units [21].

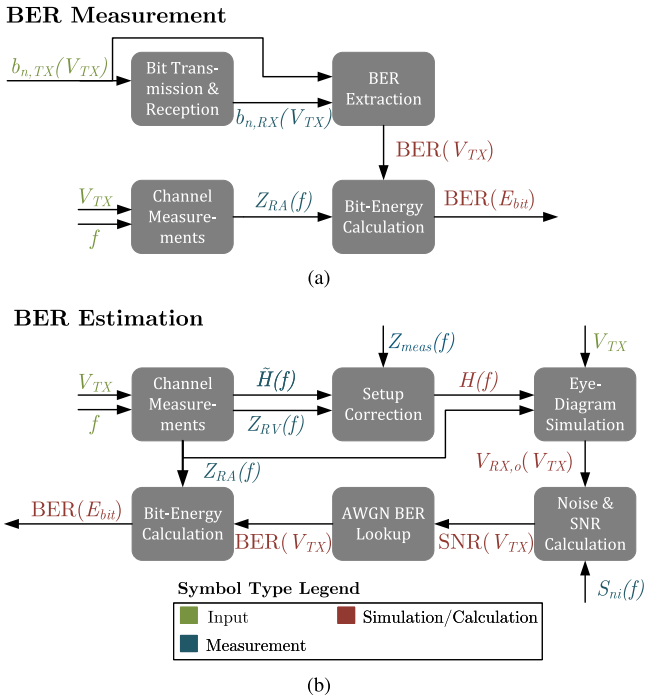

Fig. 3. In (a) the measurement and post-processing steps to obtain the bit error rate (BER) during the in-vitro experiments are shown. In (b) the BER estimation procedure, based on transfer function and impedance measurements of the intracardiac channel, is depicted.

The amplitude and phase of the transmitted signal (V_{TX}) and the received signal ($V_{RX,meas}$) were measured in two consecutive frequency sweeps. The transfer function $\tilde{H}$ was obtained by

$$\tilde{H} = \frac{V_{RX,meas}}{V_{TX}}. \tag{2}$$

The MFIA input impedance and the electrode cables (UMCX) introduced a load $Z_{meas} = (10\ \text{M}\Omega \parallel 39\ \text{pF})$ across the RX electrodes. The parallel combination of Z_{meas} (pre-dominantly capacitive) and the RX inter-electrode impedance Z_{RV} (mainly resistive) forms a low-pass filter, potentially altering $\tilde{H}$ at frequencies above 1 MHz. To correct for such setup-induced loading effects, the unloaded transfer function H was calculated from $\tilde{H}$ by

$$H = \frac{Z_{meas} + Z_{RV}}{Z_{meas}}\tilde{H} = \frac{Z_{meas} + Z_{RV}}{Z_{meas}}\frac{V_{RX,meas}}{V_{TX}}, \tag{3}$$

using a Thévenin equivalent of the intracardiac channel (see supplementary material for more details).

E. BER Estimation

An additive white Gaussian noise (AWGN) model is employed to determine the BER in simulation as shown in Fig. 3(b). In a first step, the receiver output amplitude $V_{RX,o}(V_{TX})$ is simulated as function of the transmitter amplitude V_{TX} based on the channel characteristics (H, Z_{RA} and Z_{RV}) measured in the in-vitro experiments (cf. Section II-D2). In a next step, the signal-to-noise ratio SNR(V_{TX}) is calculated from $V_{RX,o}(V_{TX})$ and the numerically approximated RMS noise amplitude $V_{no,rms}$.

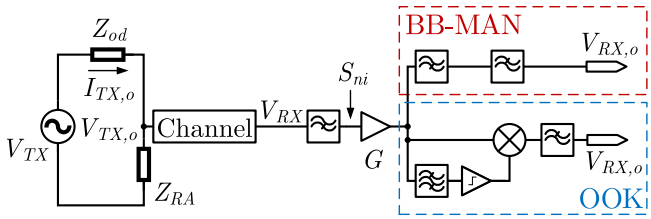

Fig. 4. Circuit schematic used for the eye-diagram simulation, the receiver noise analysis and the E_{bit} calculation.

The bit error rate BER(V_{TX}) is subsequently obtained from SNR(V_{TX}) with the help of a look-up table, containing the pre-simulated BER(SNR) values of an AWGN channel. In the last step, the BER is expressed as a function of the bit-energy E_{bit}, which is calculated based on V_{TX} and the transmitter inter-electrode impedance Z_{RA}. In the following subsections the individual steps are explained in more detail.

1) Eye Diagram Simulation: The simulation schematic shown in Fig. 4 is implemented in Simulink 10.1 (MathWorks, USA). On the transmitter side, the output impedance Z_{od} of the TX driver is included to account for loading effects introduced by Z_{RA}. The channel is modelled with the transfer function obtained during the in-vitro experiments. On the receiver side, the most critical circuits such as the input amplifier, the filters and the OOK demodulator are considered. Depending on the modulation scheme, the output signal of the receiver is periodically sampled in the middle of each bit-pulse (OOK) or each half-bit-pulse (BB-MAN), respectively. To include the effect of inter-symbol-interference, the vertical eye opening, produced by a random bit sequence (length N_{bit}= 2500), is determined and used for the subsequent SNR calculations. Representative eye diagram simulation plots are shown in the Supplement for both BB-MAN and OOK.

2) Noise Calculation: In the simulation model, noise is injected at the receiver input with a power spectral density $S_{ni}(f)$ (cf. Fig. 4). The RMS noise level $V_{no,rms}$ at the receiver output, required to determine the SNR, is numerically calculated by

$$V_{no,rms}^2 = \int_0^\infty S_{no}(f)df, \tag{4}$$

where S_{no} represents the output noise spectrum.

For the BB-MAN receiver, S_{no} can be directly obtained with linear circuit analysis by

$$S_{no,MAN}(f) = S_{ni}(f) \cdot G^2 \cdot |H_{filt}(f)|^2, \tag{5}$$

where G is the gain of the receiver and H_{filt} is the combined transfer function of the filters following amplification.

For the OOK receiver, a flat noise density is used, which is a valid assumption in the signal bandwidth around the carrier frequency f_{car} (cf. Section II-B1). Under this assumption the input and output noise densities of an ideal switching mixer are identical [22]. Thus, the receiver output noise density becomes

$$S_{no,OOK}(f) = \bar{S}_{ni,fcar} \cdot G^2 \cdot |H_{LPF,OOK}(f)|^2, \tag{6}$$

where $H_{LPF,OOK}$ represents the baseband low-pass filter at the output of the demodulator. $\bar{S}_{ni,fcar}$ is obtained by averaging S_{ni} over the signal bandwidth around f_{car}.

The input noise power spectrum S_{ni} was obtained from noise measurements of the receiver prototype (cf. Fig. 7(d)). To include thermal noise from the channel, a 240 Ω resistor was connected across the differential inputs of the receiver during the measurement.

3) E_{bit} Calculation: The energy per bit E_{bit}, for a sequence of N bits sent at a data rate f_{data}, is calculated from the instantaneous transmitted power by

$$E_{bit} = \frac{1}{N} \int_0^{\frac{N}{f_{data}}} V_{TX,o}(t) \cdot I_{TX,o}(t) dt. \tag{7}$$

The transmitter output voltage $V_{TX,o}(t)$ and current $I_{TX,o}(t)$ are obtained from the eye-diagram simulation presented in the previous subsection (cf. Fig. 4).

In the results Section, E_{bit} values are reported in decibels relative to 1 Joule, obtained by

$$E_{bit}[\text{dBJ}] = 10 \cdot \log_{10}\left(\frac{E_{bit}[\text{J}]}{1\ \text{J}}\right). \tag{8}$$

4) Simulation Conditions: To directly compare the performance of OOK and BB-MAN, the following implementation-specific confounding factors were considered. Firstly, the input noise density should be identical and the LPF cut-off frequencies should be matched for the two receivers. To meet the first condition, the receiver was designed with a white noise characteristic, since for the same data rate f_{data} the two modulation schemes operate at different frequencies. However, amplifier non-idealities, as well as 1/f-noise, can lead to a deviating noise characteristic. In addition, component tolerances and parasitic capacitances can shift the cut-off frequencies in the LPF circuits. Secondly, the capacitance of the RX electrode cables can alter the signal attenuation (cf. Section II-D2). Lastly, in the OOK receiver a first-order LPF was used, while a second-order filter was employed in the BB-MAN receiver. Although circuit simulations during the receiver development had shown, that the filter-order has a minor impact on the SNR, we included this effect for completeness.

The impact of the described effects was investigated in simulation. For each measured in-vitro configuration two corresponding BER simulations, one with effective and one with equalized receiver parameters, were performed. For the effective simulations, the noise and LPF characteristics, as measured on the receiver prototype, were used. The equalized simulations employed a white noise characteristic and a second-order LPF with cut-off frequencies precisely matched to f_{data} for both modulation schemes. In contrast to the effective simulations, the transfer function correction not only included the MFIA, but also the RX cables, since in future miniaturized electronics cabling could be minimized (cf. Section II-D2).

F. Performance Evaluation

1) Fitting BER Vs. E_{bit} Data: For each in-vitro configuration a separate BER vs. E_{bit} curve was obtained in measurement and simulation. To get a statistical representation, an averaged curve was fitted to all available data points at the same modulation scheme and data rate (see supplementary material for more details).

2) Averaging E_{bit} Data: The minimum required E_{bit} to achieve a target BER = 1e−4 was extracted individually from the BER vs. E_{bit} characteristic of each in-vitro configuration. The median and interquartile range (IQR) were then calculated over all configurations sharing the same modulation scheme and data rate.

III. Results

The raw data of the results presented in this Section are available online on the IEEE DataPort platform [23].

A. CIC-Channel Measurements

A total of 15 separate transfer functions, RA and RV impedance measurements were taken from 5 porcine hearts at three different RV electrode orientations of 0°, 30° and 60°.

1) Transfer Function: In Fig. 5(a) the median channel attenuation $|H(f)|$ is shown for hearts with and without blood. The frequency behavior in the range from 1 kHz to 5 MHz was similar for the two sample types. In Fig. 5(b) the median $|H(f)|$ for the three RV electrode orientations of 0°, 30° and 60° is depicted. For 0° and 30° the attenuation levels were almost identical. In contrast, a 1-2 dB higher attenuation was observed for 60° as compared to 0° and 30°.

2) Inter-Electrode Impedance: In Fig. 5(c) and (d) the median inter-electrode impedances ($|Z_{RA}|$ and $|Z_{RV}|$) are shown for the two groups of samples with and without blood. The impedance decreased with frequency, independent of the electrode position and whether blood was added.

B. Bit Error Rate

Each of the five in-vitro samples was measured at the four data rates at an RV electrode orientation of 0°. At RV electrode orientations of 30° and 60°, additional measurements were performed at 150 kbps and 500 kbps.

1) BER Vs. E_{bit}: In Fig. 6 the BER as a function of E_{bit} is shown separately for BB-MAN and OOK at different data rates. Both BB-MAN and OOK showed similar BER vs. E_{bit} characteristics over the entire data rate range. The mean BER decreased by 2 orders of magnitude for an increase of E_{bit} by 4-6 dB. Depending on the data rate and modulation scheme, the measurements showed a mean offset between -1 dB to 3 dB along the E_{bit} axis.

2) E_{bit} Vs. Data Rate: In Fig. 7(a) and (b) the median and IQR of the minimum required E_{bit}, to achieve a target BER of 1e−4, are shown for BB-MAN and OOK, respectively.

For the BB-MAN measurements a median E_{bit} in the range from -115 dBJ to -113 dBJ (3-5 pJ) was obtained and no clear trend with data rate could be observed. The simulations predicted no frequency dependence for the effective receiver and a 2 dB increase from 75-500 kbps under equalized conditions. In the simulation the target BER was achieved with 1-2 dB (effective) and 2-4 dB (equalized) lower E_{bit} values compared to the measurements.

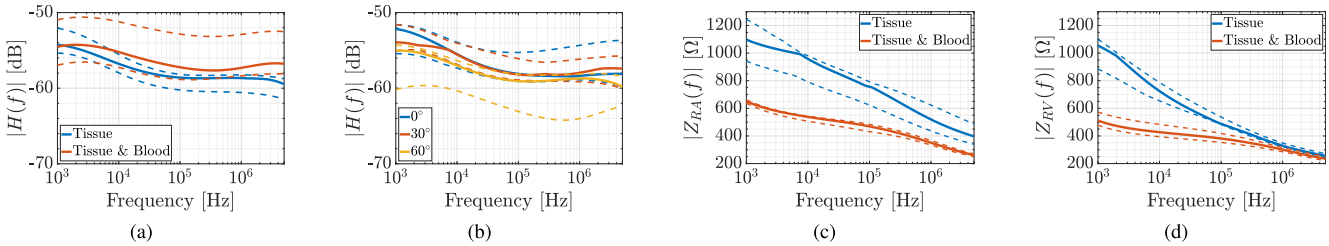

Fig. 5. Channel characteristics observed during in-vitro experiments. The median attenuation and interquartile range (IQR) for different (a) channel types and (b) RV electrode orientations are shown as function of the frequency. The median and IQR of the impedance magnitude are shown for the RA (c) and the RV (d) electrodes.

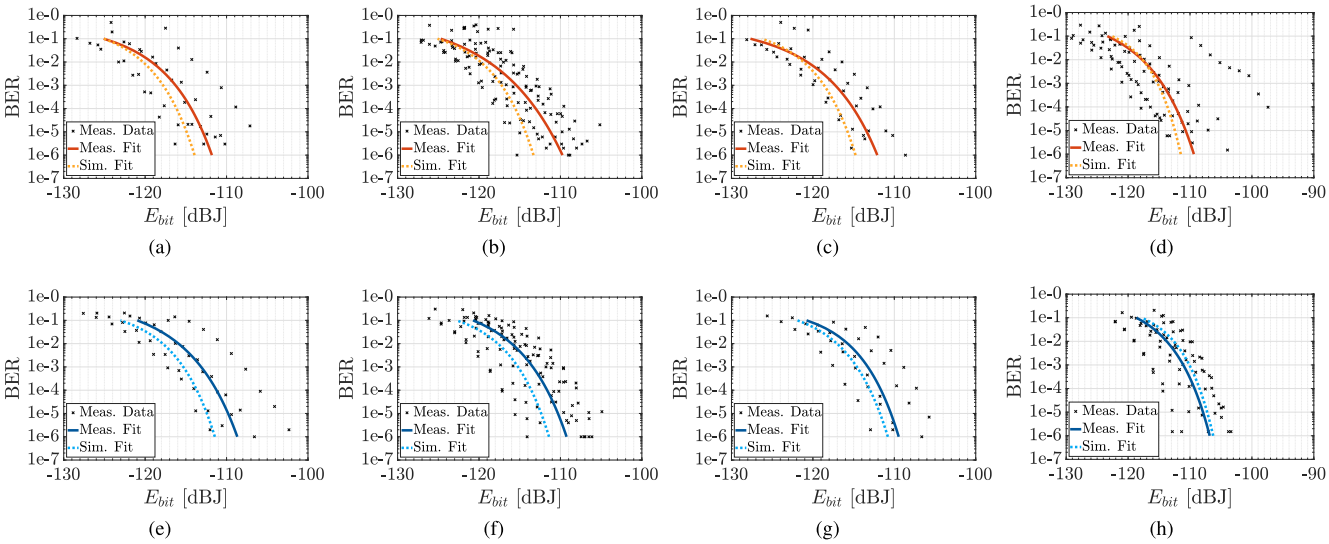

Fig. 6. Bit error rate (BER) vs. energy per bit (E_{bit}) performance of the prototype dual-chamber LLPM for (a)-(d) BB-MAN and (e)-(h) OOK modulation. Four different data rates of 75 kbps (a, e), 150 kbps (b, f), 300 kbps (c, g), and 500 kbps (d, h) were measured.

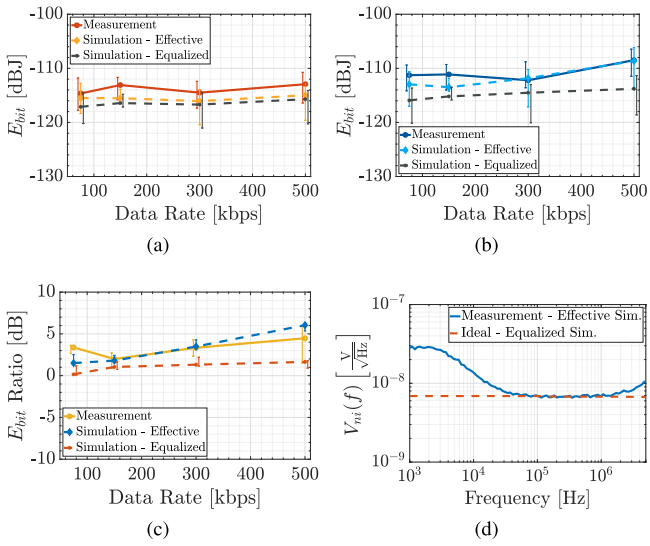

Fig. 7. Minimum required bit-energy (E_{bit}) to achieve a bit error rate (BER) of 1e−4 for (a) BB-MAN and (b) OOK. In (c) the E_{bit} ratio between OOK and BB-MAN at the same target BER = 1e−4 is shown. In (d) the measured and the idealized receiver input noise density are shown, which were used for the effective and equalized simulations, respectively.

For OOK the median E_{bit}, obtained in the measurements, was between -112 dBJ and -108.5 dBJ (6-14 pJ), increasing by 3 dB at 500 kbps compared to the lower data rates. The simulations of the effective receiver predicted a 5 dB increase from 150-500 kbps. The simulations of the equalized receiver showed a reduced dependence of E_{bit} on data rate, increasing by only 2.5 dB from 75-500 kbps. The target BER was achieved with 0-2.5 dB (effective) and 2.5-5 dB (equalized) lower E_{bit} values, when comparing the simulations to the measurements.

3) Modulation Scheme Comparison: In Fig. 7(c) the median and IQR of the E_{bit} ratio between OOK and BB-MAN at a target BER = 1e−4 are shown as a function of the data rate. In the measurements a 2-4.5 dB higher bit-energy was required for OOK compared to BB-MAN, with the performance difference increasing at higher data rates. A similar characteristic was observed in the simulations of the effective receiver, showing a monotonic increase of the E_{bit} ratio from 1.5 dB to 6 dB from 75-500 kbps. The simulations under equalized conditions predicted a comparable performance of the two modulation techniques at 75 kbps and a performance advantage for BB-MAN of 1-2 dB for data rates from 150-500 kbps.

Fig. 7(d) shows the measured input-referred noise density S_{ni} of the receiver prototype, which has been used as an input for

TABLE I
PERFORMANCE COMPARISON WITH PREVIOUS CONDUCTIVE INTRABODY COMMUNICATION PROTOTYPES

Publication	**Bereuter et al. [9]**	**Khaleghi et al. [12]**	**Maldari et al. [15]**	**Yuk et al. [25]**	**This Work**	**This Work**
Modulation	PPM	CIS	OOK	Direct Digital 3-Level Polar RZ	BB-MAN	OOK
Measurement Type	In-Vivo	In-Vitro	Simulation	In-Vivo/In-Vitro	In-Vitro	In-Vitro
Channel	Porcine Heart/Blood	Saline Phantom	Porcine Heart/Blood	Rat Brain/Phosphate-Buffered Saline	Porcine Heart/Blood	Porcine Heart/Blood
Electrode (El.) Type	Epicardial Needles without Blood Contact	Caps at Opposite Ends of Cylinder LLPM Capsule	Disk/Cylinder at Opposite Ends of LLPM Capsule	Rectangular Copper Microelectrode Plate	Epicardial Needles with Blood Contact	Epicardial Needles with Blood Contact
El. Distance [mm]	10–15	27	33	TX:N.A. RX:40	15	15
El. Area [mm^2]	2.5–4.5	51	4/22	TX:0.07–0.3 RX:79	13	13
Attenuation [dB][a]	53.5	57	60-70	66/33	58.5	58.5
$\mathbf{Z_{RA}}$ **[Ω]**	600	90	1000	N.A.	555	385
Frequency [MHz]	1	0.01-10	4	DC-20	0.001-0.3	1.5
Data Rate [kbps]	41.7	8	2	16700	150	150
BER	>2e−4	2.2e−3	1e-4	N.A./1e-9	1e−4	1e−4
$\mathbf{E_{bit}}$ **[nJ]**	3.1	1.4	0.05–0.5	0.034	0.005	0.008
$\mathbf{P_{TX}}$ **[nW]**[b]	310	140	5–50	3.4	0.5	0.8
$\mathbf{t_{message}}$ **[ms]**[b]	2.3	12.5	50	0.006	0.7	0.7
RX Input Noise [$\frac{\mathrm{nV}}{\sqrt{\mathrm{Hz}}}$]	6.5	N.A	N.A.	12.4	7	7
RX $\mathbf{P_{cir}}$ **(Analog) [mW]**	>465	>230[c,d]	0.018	0.062	152[d]	191[d]
TX $\mathbf{P_{cir}}$ **(Analog) [mW]**	>360	0.025	N.A.	0.57	97[d,e]	97[d,e]
Technology	Discrete	Discrete	180 nm CMOS	110 nm CMOS	Discrete	Discrete

[a] At 1 MHz.[b]
[b] $P_{TX} = N_{bit} E_{bit} f_{HR}$, for $N_{bit} = 100$ bits transmitted per heart cycle at an average heart rate of $f_{HR} = 60$ beats per minute and $t_{message} = \frac{N_{bit}}{f_{data}}$
[c] Calculated based on typical data sheet values of the components shown in the circuit schematic provided in [12].
[d] For a supply voltage of $V_{DD} = 5$ V.
[e] Only contribution of the TX driver.

the effective BER simulations. The flat noise density, used for the equalized simulations, is also shown for comparison.

IV. DISCUSSION

This study found that reliable intracardiac communication is feasible at very low E_{bit} levels, using simple modulation techniques. With an optimized receiver design a BER = 1e−4 was achieved, under realistic channel conditions, with a median E_{bit} in the range of 3-16 pJ for data rates from 75-500 kbps. A good agreement between the BER measurements and simulations was found. These results suggest that the BER vs. E_{bit} performance is well predicted by the presented system model, which considers the attenuation and the impedance of the intracardiac channel, as well as noise arising from the receiver electronics and the cardiac tissue.

A. Implications for CIC-Transceiver Design

1) Power Consumption Budget: A future dual-chamber LLPM could potentially achieve AV-sequential pacing by exchanging less than 100 synchronization bits per heart beat [9]. Under this assumption, the presented system would achieve an average transmitted power $P_{TX} < 1$ nW, for a data rate of 150 kbps assuming a typical average heart rate of 60 bpm. These results indicate that for a miniaturized transceiver with comparable performance, there is a considerable margin to increase the transmitter amplitude V_{TX} (and thus P_{TX}) compared to the values used in this work without significantly affecting the overall 2-5 μW power consumption of a LLPM. This is promising for two reasons. Firstly, this may guarantee reliable communication even in the case of time-dependent signal attenuation and long-term drift of channel properties, which have to be expected in a living beating heart [10], [12], [24]. Specifically, in-vivo experiments on porcine hearts have found variations in attenuation as high as ± 5 dB at 1 MHz relative to the time average [10], [12]. Therefore, the reported values for P_{TX} and E_{bit}, which were measured under stationary conditions, would need to be increased by up to a factor of 5 dB to guarantee similar communication performance in a beating heart. Secondly, a larger V_{TX}, for a given channel attenuation, allows to increase the receiver noise level, while keeping the SNR and the BER constant. This is beneficial, since in sensitive receivers a significant part of the power consumption is devoted to achieve the low noise performance.

Ultimately, a power-efficient transceiver should minimize the total power consumption P_{tot}, which is the sum of the transmitted power P_{TX} and the circuit power consumption P_{cir} (cf. equation (1)). In addition, to maximize the longevity of a dual-chamber LLPM, i.e. the time period until either of the two devices needs to be replaced due to battery depletion, the power consumption of the atrial and the ventricular device should ideally be matched. The presented system model can help to achieve both of these goals, during the design of future power-optimized transceivers, as it provides an accurate estimation for P_{TX} as function of the most important system parameters.

2) Modulation Scheme Selection: For all listed prototypes in Table I, the power consumption of the transceiver electronics P_{cir} exceeds the transmitted power P_{TX} by orders of magnitude, since for LLPM synchronization only a small amount of bits need to be communicated per heart cycle. In addition, the presented receiver, as well as the ones in Refs. [9] and [12], have a

power consumption ($P_{cir} > 150$ mW) that significantly exceeds the power budget of a LLPM, due to their implementation based on discrete components. Therefore, future work should focus on minimizing P_{cir}, by integrating the electronics on a single chip. Results from recent integrated receivers for intra-body communication indicate the potential power consumption savings of miniaturization. Specifically, in Refs. [15] and [25], shown in table I for comparison, similar E_{bit} performance was achieved, for comparable channel conditions and communication parameters, at a power consumption in the order of a few tens of microwatts.

To minimize P_{cir}, the selection of the modulation scheme should also be carefully considered. This study suggests that BB-MAN and OOK are promising candidates for reducing P_{cir}, since good communication performance was achieved and the corresponding transceivers can be implemented with a minimal amount of circuit blocks. Modulation schemes such as PPM or CIS, which could be more suitable for P_{TX}-limited systems, but also increase circuit complexity and bandwidth requirements, may not represent a power-efficient choice.

We observed a 2-6 dB performance advantage for BB-MAN over OOK modulation. The difference increased with higher data rates in both, the measurements and the effective receiver simulations (cf. Fig. 7(c)). Additional simulations with equalized receiver parameters were performed to eliminate implementation-specific confounding factors such as non-flat noise characteristics, RX cable capacitance and LPF mismatch. Based on these results, the data rate dependence of the effective E_{bit} ratio, is most probably explained by the increase of the receiver input noise density above 1.5 MHz (cf. Fig. 7(d)). The increased noise density manifests as an SNR reduction of the OOK signal at 300-500 kbps and a corresponding increase in the E_{bit} ratio. The remaining performance advantage for BB-MAN, of 1-2 dB above 75 kbps, can be explained by the frequency characteristics of the communication channel. The relatively flat transfer functions do not strongly favor either of the two modulation techniques (cf. Fig. 5(a)). However, the lower impedance of myocardial tissue and blood for higher frequencies (cf. Fig. 5(c)), increases the transmitter current (and thus E_{bit}) for OOK due to the higher communication frequency as compared to BB-MAN. A baseband approach such as BB-MAN may therefore be favored over OOK, since the performance advantage in E_{bit} increases the available power budget of the electronics. In addition, it is expected that a baseband system can further reduce power consumption, since no (de)modulation circuits are necessary and the required bandwidth will be smaller for an anticipated data rate.

3) Impact of 1/f-Noise: The receiver has a 1/f-noise characteristic (below $\sim$16 kHz) affecting the BB-MAN signal, which extends to frequencies as low as 1 kHz. The impact of different receiver noise characteristics on the bit-energy (E_{bit}) was analyzed in simulation (cf. Section II-E4). As shown in Fig. 7(a), the E_{bit} results for BB-MAN were increased by 0.4-2 dB, due to the effect of 1/f-noise, compared to a receiver with a pure white noise characteristic. The largest effect was observed at the smallest data rate of 75 kbps, since the relative contribution of the 1/f-noise to the total RMS noise power increases, if the overall bandwidth decreases. However, for a custom-designed receiver, using a CMOS input amplifier with an active current consumption in the order of a few tens of micro-amperes, the 1/f-corner frequency may be reduced below 10 kHz [26], [27]. Thus, the effect of 1/f-noise on CIC performance can most probably be minimized for data rates above 50-100 kbps with an optimized receiver design.

B. Selection of Communication Parameters

1) Safety of CIC: To avoid accidental pacing, the half-waves of the sinusoidal carrier (OOK) and the bit-pulses (BB-MAN) need to be below the myocardial capture threshold, which, for LLPMs, is typically in the range of 240 μs at an amplitude of $\sim$0.5 V [28]. In this work, a maximum unipolar pulse duration of $<$20 μs and transmitter amplitude of $<$0.2 V were used. Considering Lapique's equation and typical chronaxie and rheobase values, the expected capture threshold is above 3 V for a 20 μs rectangular pulse, [29]. Consequently, CIC seems feasible without invoking myocardial capture assuming a data rate above 50 kbps and a carrier frequency above 40 kHz.

2) CIC-Channel Properties: The minimum E_{bit} for a BER $=$ 1e$-$4 increased moderately with the data rate. This can be explained by the decrease of the transmitter inter-electrode impedance with increased frequency. As this trend is small, the selection of the optimal communication frequency and data rate should not be purely driven by the channel properties, but include electronic design considerations, as well. In terms of the transceiver a trade-off for increasing the data rate has to be made: On the one hand, an increase shortens the duration of a communication message $t_{message}$, allowing to decrease the average electronic power consumption, since the total active time can be reduced. On the other hand, the transceiver needs to have a larger bandwidth, most probably increasing the instantaneous power consumption.

C. Variation of Channel Attenuation

We observed identical attenuation as function of the frequency for the three RV electrode orientations. In addition, the absolute level of attenuation was similar for 0° and 30° and increased slightly for 60°. These results agree with recent simulations, which reported a small variation of the attenuation for angles up to 60° and a steep increase for even larger angles [10]. A low attenuation variation with relative orientation of the transmitter and receiver is beneficial for the dual-chamber LLPM due to two reasons. Firstly, it is challenging to implant a device at a precise location with a pre-specified orientation due to the limited maneuverability of catheter-based implantation tools. Secondly, patient anatomy and the pacing threshold also play an important role in the selection of a suitable implantation site. Furthermore, the attenuation is less sensitive to the angle than time-dependent variations, which are on the order of ± 5 dB as previously discussed (cf. IV-A1). In conclusion, moderate angles between the two LLPMs, should not significantly impede the system design. In any case, channel altering attenuation due to variations in device distance, channel properties, as well as time-dependence due to the cardiac cycle and long-term drift, have to be considered.

D. Future Work

Future work should focus on reducing the circuit power consumption by integrating the transceiver electronics into an ASIC. A detailed analysis of duty-cycled transceiver operation on pacing performance will be crucial, to minimize the active time and thus to reduce the average power consumption at the system level. The authors are currently working on a low-power CIC-transceiver ASIC based on the presented prototypes. This will allow to validate the results of this study in a realistic in-vivo setting, by incorporating the electronics in a fully-implantable LLPM prototype.

V. Limitations

The usage of porcine in-vitro samples extracted after death is a limitation of this work. However, the time-averaged channel characteristics, measured in earlier in-vivo experiments, are similar to the results obtained during the in-vitro experiments of this and previous work [10], [11]. In addition, the channel parameters were constant over time due to the non-beating heart. The time-variation of attenuation, however, is considered to not fundamentally change the findings of this study, as cardiac motion happens on a much slower time scale compared to the data rates considered here. Moreover, in a typical dual-chamber operation the communication window would take place at a relatively fixed time point relative to the cardiac cycle. Based on this consideration, it is expected that the variation over time is significantly low and not prohibitive.

Potential disturbances due to the intrinsic electrical signals of the heart could not be studied. However, signals from cardiac activity have dominant energy contents at frequencies far below 100 Hz, falling outside the investigated communication bandwidth from 10 kHz to 5 MHz. In addition, the receiver prototype included multiple high-pass filter stages designed to reduce physiological signals to negligible levels. The experiments used symmetric epicardial needle electrodes with simultaneous contact to myocardium and blood, while commercial LLPMs feature tip and ring electrodes, which are predominantly in contact with either tissue or blood, respectively. In addition, the electrode arrangement was simplified compared to the possible relative orientations of two endocardial LLPMs in three spatial dimensions. However, these differences are unlikely to significantly modify the BER results, since the attenuation and impedance measurements were in good agreement with previous in-vivo experiments using more realistic endocardial LLPM capsules [11]. Furthermore, endocardial experiments would have required miniaturized electronics, which were beyond the scope of this study. However, further work is planned to develop an integrated transceiver (cf. Section IV-D).

VI. Conclusion

A model for estimation of the BER as function of the most important system parameters was validated during in-vitro experiments and could serve as a basis for the design of future power-optimized transceivers. Reliable LLPM synchronization is feasible at very low transmitted power, given that only a few bits will need to be exchanged per cardiac cycle in a typical clinical setting. The power consumption of the synchronization process is most likely dominated by the electronics, even for a future miniaturized transceiver. Therefore, simple modulation techniques such as baseband transmission with Manchester encoding or On-Off-Keying, which can be implemented with minimal hardware resources, seem to be preferable in a future power-optimized transceiver. Ultimately, a baseband communication approach might be favored over OOK, due to the more efficient cardiac signal transmission and reduced transceiver complexity.

Acknowledgment

The authors would like to thank M. Hofmann for his support during the in-vitro experiments, A. Macpherson for his assistance in mechanical manufacturing and Act-Inno AG for providing the testing facilities.

References

[1] H. G. Mond and A. Proclemer, "The 11th world survey of cardiac pacing and implantable cardioverter-defibrillators: Calendar year 2009-A world society of arrhythmia's project," *Pacing Clin. Electrophysiol.*, vol. 34, no. 8, pp. 1013–1027, Aug. 2011.

[2] F. V. Tjong and V. Y. Reddy, "Permanent leadless cardiac pacemaker therapy," *Circulation*, vol. 135, no. 15, pp. 1458–1470, Apr. 2017.

[3] E. O. Udo *et al.*, "Incidence and predictors of short- and long-term complications in pacemaker therapy: The FOLLOWPACE study," *Heart Rhythm*, vol. 9, no. 5, pp. 728–735, May 2012.

[4] A. Haeberlin *et al.*, "Leadless pacemaker implantation quality: Importance of the operator's experience," *EP Eur.*, vol. 22, no. 6, pp. 939–946, Jun. 2020.

[5] F. Neugebauer *et al.*, "Leadless atrioventricular synchronous pacing in an outpatient setting: Early lessons learned on factors affecting atrioventricular synchrony," *Heart Rhythm*, vol. 19, pp. 748–756, Dec. 2021.

[6] L. Bereuter *et al.*, "Leadless dual-chamber pacing," *JACC Basic Transl. Sci.*, vol. 3, no. 6, pp. 813–823, Dec. 2018.

[7] P. Bose, A. Khaleghi, M. Albatat, J. Bergsland, and I. Balasingham, "RF channel modeling for implant-to-implant communication and implant to subcutaneous implant communication for future leadless cardiac pacemakers," *IEEE Trans. Biomed. Eng.*, vol. 65, no. 12, pp. 2798–2807, Dec. 2018.

[8] V. De Santis and M. Feliziani, "Intra-body channel characterization of medical implant devices," in *Proc. EMC Eur. 2011 York - 10th Int. Symp. Electromagn. Compat.*, 2011, pp. 816–819.

[9] L. Bereuter *et al.*, "Leadless cardiac resynchronization therapy: An in vivo proof-of-concept study of wireless pacemaker synchronization," *Heart Rhythm*, vol. 16, no. 6, pp. 936–942, Jun. 2019.

[10] L. Bereuter *et al.*, "Fundamental characterization of conductive intracardiac communication for leadless multisite pacemaker systems," *IEEE Trans. Biomed. Circuits Syst.*, vol. 13, no. 1, pp. 237–247, Feb. 2019.

[11] M. Maldari, M. Albatat, J. Bergsland, Y. Haddab, C. Jabbour, and P. Desgreys, "Wide frequency characterization of intra-body communication for leadless pacemakers," *IEEE Trans. Biomed. Eng.*, vol. 67, no. 11, pp. 3223–3233, Nov. 2020.

[12] A. Khaleghi, R. Noormohammadi, and I. Balasingham, "Conductive impulse for wireless communication in dual-chamber leadless pacemakers," *IEEE Trans. Microw. Theory Tech.*, vol. 69, no. 1, pp. 443–451, Jan. 2021.

[13] G. Kim and Y. Park, "Suitable combination of direct intensity modulation and spreading sequence for LIDAR with pulse coding," *Sensors*, vol. 18, no. 12, Nov. 2018.

[14] Y. Fujiwara, "Self-synchronizing pulse position modulation with error tolerance," *IEEE Trans. Inf. Theory*, vol. 59, no. 9, pp. 5352–5362, Sep. 2013.

[15] M. Maldari, C. Jabbour, Y. Haddab, and P. Desgreys, "Ultra-low power system for atrioventricular synchronization using leadless pacemakers," *URSI Radio Sci. Bull.*, vol. 2021, no. 376, pp. 9–23, 2021.

[16] H. Cho *et al.*, "A 79 pJ/b 80 mb/s full-duplex transceiver and a 100 kb/s super-regenerative transceiver for body channel communication," *IEEE J. Solid-State Circuits*, vol. 51, no. 1, pp. 310–317, Jan. 2016.

[17] V. D. Rezaei and K. Entesari, "A fully on-chip 80-pJ/b OOK super-regenerative receiver with sensitivity-data rate tradeoff capability," *IEEE J. Solid-State Circuits*, vol. 53, no. 5, pp. 1443–1456, May 2018.
[18] V. Mangal and P. R. Kinget, "An ultra-low-power wake-up receiver with voltage-multiplying self-mixer and interferer-enhanced sensitivity," in *Proc. IEEE Cust. Integr. Circuits Conf.*, Apr. 2017, pp. 1–4.
[19] C. Ma, C. Hu, J. Cheng, L. Xia, and P. Y. Chiang, "A near-threshold, 0.16 nJ/b OOK-Transmitter with 0.18 nJ/b noise-cancelling super-regenerative receiver for the medical implant communications service," *IEEE Trans. Biomed. Circuits Syst.*, vol. 7, no. 6, pp. 841–850, Dec. 2013.
[20] G. A. Alvarez-Botero, Y. K. Hernandez-Gomez, C. E. Tellez, and J. F. Coronel, "Human body communication: Channel characterization issues," *IEEE Instrum. Meas. Mag.*, vol. 22, no. 5, pp. 48–53, Oct. 2019.
[21] M. A. Callejon, J. Reina-Tosina, D. Naranjo-Hernandez, and L. M. Roa, "Measurement issues in galvanic intrabody communication: Influence of experimental setup," *IEEE Trans. Biomed. Eng.*, vol. 62, no. 11, pp. 2724–2732, Nov. 2015.
[22] B. Razavi, "Chapter 6 Mixers," in *RF Microelectronics*, 2nd ed. Upper Saddle River, NJ, USA: Pearson Education, 2012, pp. 343–436.
[23] A. Ryser *et al.*, "In-vitro measurements of porcine conductive intracardiac channel properties," 2022. [Online]. Available: https://dx.doi.org/10.21227/c0ew-c088
[24] R. Noormohammadi, A. Khaleghi, J. Bergsland, and I. Balasingham, "Conductive backscatter communication for dual-chamber leadless pacemakers," *IEEE Trans. Microw. Theory Tech.*, vol. 70, no. 4, pp. 2442–2450, Apr. 2022.
[25] B. Yuk, B. Kim, S. Park, Y. Huh, and J. Bae, "An implantable body channel communication system with 3.7-pJ/b reception and 34-pJ/b transmission efficiencies," *IEEE Solid-State Circuits Lett.*, vol. 3, pp. 50–53, 2020.
[26] M. Manghisoni *et al.*, "Technologies for detector front-end applications," *Proc. IEEE Nucl. Sci. Symp. Conf. Rec.*, pp. 955–959, 2005.
[27] M. Manghisoni, L. Ratti, V. Re, V. Speziali, and G. Traversi, "Low-noise design issues for analog front-end electronics in 130 nm and 90 nm CMOS technologies," in *Proc. 12th Work. Electron. LHC Futur. Exp. LECC*, 2007, pp. 483–487.
[28] G. Z. Duray *et al.*, "Long-term performance of a transcatheter pacing system: 12-Month results from the micra transcatheter pacing study," *Heart Rhythm*, vol. 14, no. 5, pp. 702–709, May 2017.
[29] S. Coates and B. Thwaites, "The strength-duration curve and its importance in pacing efficiency: A. study of 325 pacing leads in 229 patients," *Pacing Clin. Electrophysiol.*, vol. 23, no. 8, pp. 1273–1277, Aug. 2000.

Adrian Ryser received the B.Sc and M.Sc. degrees in physics from ETH Zurich, Zurich, Switzerland, in 2013 and 2016, respectively. He is currently working toward the Ph.D. degree in biomedical engineering with the SITEM Center for Translational Medicine and Biomedical Entrepreneurship and the Department of Cardiology, Bern University Hospital, Bern. From 2017 to 2020, he worked as an analog IC design engineer at ON Semiconductor, Dübendorf and AMS International AG, Rapperswil and Knowles Electronics GmbH, Rapperswil. His research interests include low-power ASIC design for medical implants, intrabody communication, and cardiovascular engineering.

Tobias Schmid received the B.Sc. degree in electrical engineering from the University of Applied Sciences HSR (OST), Rapperswil, Switzerland, in 2020. He is currently working toward the M.Sc. degree in human technology in sports and medicine at the German Sports University GSU in Cologne, Germany.

Lukas Bereuter received the B.Sc. degree in systems engineering from the University of Applied Sciences ZHAW, Winterthur, Switzerland, in 2012, and the M.Sc. and Ph.D. degrees in biomedical engineering from the University of Bern, Bern, Switzerland, in 2014 and 2018, respectively. He is currently performing research and developing a medical device in the field of urology.

Jürgen Burger received the diploma and doctoral degree in physics from the University Erlangen-Nuremberg, Nuremberg, Germany, in 1987 and 1993, respectively. He is a Full Professor for Translational Medicine and Entrepreneurship at the Faculty of Medicine of the University of Bern, Bern, Switzerland. He is also the Director of the SITEM Center for Translational and Biomedical Entrepreneurship in Medicine. The focus of his research is on bringing innovative treatment methods and therapeutic/diagnostic systems into clinical application. A special focus is on intelligent implants and surgical instruments in combination with pharmaceutical products.

Tobias Reichlin received the M.D. degree from the Faculty of Medicine, University of Basel, Basel, Switzerland, in 2004. He is board certified in internal medicine and cardiology. He was trained in cardiac electrophysiology from the Harvard Medical School, Boston, USA, and the University of Basel. In 2018, he was appointed as a Full Professor of cardiology and is the Head of Cardiac Electrophysiology with the University of Bern and with the University Hospital Bern, Bern, Switzerland.

Thomas Niederhauser (Member, IEEE) received the Diploma degree in electrical engineering and information technology from the Bern University of Applied Sciences (BFH), Biel, Switzerland, in 2007, and the M.Sc. and Ph.D. degrees in biomedical engineering from the University of Bern, Bern, Switzerland, in 2009 and 2014, respectively. He is currently a Professor for biomedical signal processing and control and the Head of the Institute for Human Centered Engineering, BFH. His translational research aims at the development of novel technologies for the recording, monitoring and recovery of physiologic functions. In particular, he focuses on the design of low-power hardware and signal processing algorithms for smart active medical devices intended for cardiac rhythm management, the monitoring of vital signs on (neonatal) intensive care units and dental treatments.

Andreas Haeberlin received the M.D. degree from the University of Bern, Bern, Switzerland, in 2009, and the Ph.D. degree in 2014. He received additional degrees in statistics and entrepreneurship and was trained in electrophysiology in Bordeaux, France. He is working as a Clinical Invasive Electrophysiologist and is Research Group Head at the Bern University Hospital, and a Lecturer with the University of Bern. His research interests include translational electrophysiology, in particular related to novel devices for the diagnosis and treatment of cardiac arrhythmias. He is a member of the Swiss Society of Cardiology, the European Society of Cardiology, and the European Heart Rhythm Association.